

Evolution of Microstructure and Relaxor Ferroelectric Properties in



R. Kumar^{1,2}, K. Asokan³, S. Patnaik² and B. Birajdar¹

¹*Special Centre for Nano Sciences, Jawaharlal Nehru University, New Delhi, India*

²*School of Physical Sciences, Jawaharlal Nehru University, New Delhi, India*

³*Materials Science Division, Inter University Accelerator Centre, New Delhi, India.*

Abstract

We report a study on a series of lanthanum doped barium stannate-titanate (LBTS) ceramics towards correlating their microstructure with ferroelectric properties. The samples were prepared by solid state reaction technique and the XRD analysis indicated predominantly single phase microstructure. Scanning Electron Microscopy revealed that while a low La doping of 1 atomic % yielded inhibited grain growth in 1LBTS, higher amounts of La doping yield larger leafy grains. This peculiar grain growth and microstructure evolution could be attributed to the combination of the following two competing factors: (i) suppression of O vacancies due to La doping leading to grain growth inhibition and (ii) enhancement of mechanism leading to nucleation and growth of 2-D (leafy) grains for La doping higher than 2 atomic % due to eutectic phenomena. Dielectric permittivity measurements indicate that addition of La enhances diffused phase transition in BTS, but its frequency dependence is observed only at 2 atomic % La doping. This signature relaxor behaviour and the increase in the intensity of a particular Raman peak with La doping, as well as non-saturated PE hysteresis loops confirm the presence of polar nano-regions for 2 and 3 atomic % La doped BTS. However significant enhancement in dielectric permittivity could not be achieved due to reduced grain size.

Keywords: ferroelectrics; solid state reaction; dielectric response; microstructure; scanning electron microscopy; Raman spectroscopy.

E-mail: birajdar@mail.jnu.ac.in

1. Introduction

Encompassing several potential applications, the barium titanate (BaTiO_3) based relaxor ferroelectric materials have attracted considerable attention in the recent past [1]. In particular, relaxors are potential materials for capacitors that generally require high and frequency independent dielectric constant over a broad range of temperature [2]. Apart from being environment-friendly, the properties of BaTiO_3 (BTO) ceramics are tunable to such requirements by suitable substitutions at Ba and Ti sites. By definition, relaxor ferroelectrics are characterized by broad maxima in the temperature dependent dielectric permittivity that shifts to higher temperature with increasing frequency [3-4]. This phenomenon was first evidenced in $\text{Ba}(\text{Ti}_{1-x}\text{Sn}_x)\text{O}_3$ by Smolenskii et al. (in 1954) and is currently ascribed to the development of polar nano regions (PNRs) [5-6]. This is in contrast to macroscopic polarized domains in pure BaTiO_3 that exhibit sharp dielectric peak at paraelectric (cubic) to ferroelectric (tetragonal) phase transition ($T_c \sim 403$ K) [7]. Several reports substantiate a diffused phase transition in $\text{Ba}(\text{Sn}_x\text{Ti}_{1-x})\text{O}_3$ that achieves a complete relaxor characteristics for $x \sim 0.30$ [8]. On the other hand, A site substituted $\text{La}_z\text{Ba}_{1-z}\text{Ti}_{1-z/4}\text{O}_3$ exhibits record high dielectric constant ($\sim 25,000$) alongwith exceptional electromechanical properties [9-10]. This substitution of La^{3+} in place of Ba^{2+} is linked to the creation of B-site vacancies for charge compensation. Thus, heterovalent as well as homovalent substitutions at A site (La) and B site (Sn) can be used towards tuning relaxor properties by controlling microstructure and phase segregation [9]. In this communication, we report the microstructure formation in $(\text{Ba}_{1-z}\text{La}_z)(\text{Ti}_{0.80}\text{Sn}_{0.20})\text{O}_3$ using scanning electron microscopy (SEM) and have tried to correlate it with relaxor ferroelectric properties. Furthermore, co-doping of Sn and La in Barium Titanate has been investigated using Raman Spectroscopy to study the impact of La addition on relaxor behavior.

2. Experimental Technique

The ceramic samples were prepared by conventional solid state reaction technique with starting materials BaCO_3 , La_2O_3 , TiO_2 and SnO_2 with purity $\geq 99\%$ were purchased from Sigma Aldrich. They were mixed according to the stoichiometric ratio to obtain nominal compositions of $(\text{Ba}_{1-z}\text{La}_z)(\text{Ti}_{0.80}\text{Sn}_{0.20})\text{O}_3$ ($z = 0.0, 0.01, 0.02$ and 0.03). In this manuscript these compositions are denoted as BTS, 1LBTS, 2LBTS, 3LBTS respectively. After 35 hrs electric grinding, the mixed powder was pressed into pellets of diameter 10 mm and thickness about 1 to 1.5 mm. Optimum calcination conditions were found to be 4 hrs at 1473 K for BTS and 8 hours at 1523 K for all LBTS samples. The calcined pellets were then reground and pressed into pellets of 10 mm diameter. Optimum sintering conditions were found to be 3 hrs at 1653 K for BTS and 4 hrs at 1673 K for LBTS samples except for 3LBTS which was sintered for 9 hrs. All sintering was done in presence of air in alumina crucible that resulted in highly densified ceramics. The XRD patterns of the samples were obtained with *Rigaku* diffractometer using Cu-K_α radiation. The diffractometer was operated at voltage 30 kV and current 20 mA with the scanning speed of $4^\circ/\text{min}$ for the diffraction angle 2θ in the range of $20\text{-}80^\circ$. Secondary electron images of the gold coated pellets were acquired using ZEISS EV40 scanning electron microscope (SEM). Raman spectra were acquired at room temperature over a wavenumber range of $50 - 1200 \text{ cm}^{-1}$ using Raman Spectrometer (Enspectr Enhanced spectroscopy, USA) with a green excitation light source of 532 nm line. The dielectric measurements were done using Agilent E4980A Precision LCR meter. It was carried out as a function of frequency of the applied ac field (range 25Hz–1MHz) under zero dc bias over a temperature range from 80 K to 350 K. The temperature was controlled with accuracy 1 K by using a programmable temperature controller (Lake Shore 325). To prevent electrical breakdown along the edge of the pellets and also to avoid fringing effects,

only one side of the pellets was fully coated with silver paste. The other side of the pellets was partially (70-80% diameter) coated. The real part of dielectric constant (ϵ') was calculated from the relation $\epsilon' = Ct/\epsilon_0 A$ where C , ϵ_0 , t and A are the capacitance, permittivity of free space, thickness and coated area of the sample respectively. The Polarization versus Electric field (PE) loop for all the compositions is recorded at a frequency of 50 Hz by applying a maximum electric field of 30 kV/cm at room temperature.

3. Results and Discussion

Room temperature X-ray powder diffraction pattern of $(\text{Ba}_{1-z}\text{La}_z)(\text{Ti}_{0.80}\text{Sn}_{0.20})\text{O}_3$ with ($z=0.00, 0.01, 0.02$ and 0.03) sintered ceramics are shown in Fig.1. XRD patterns of BTS and LBTS samples are in agreement with JCPDS Card No. 62-0356. Further, in agreement with existing reports, BTS and LBTS samples show cubic structure with space group $\text{Pm}\bar{3}\text{m}$ [11-12]. Extra peaks due to impurities were not found in the XRD patterns, indicating predominant single phase formation for all the prepared samples. Inset of Fig.1 shows the enlarged view of XRD pattern in the range ($2\theta = 37\text{--}47^\circ$) to depict the right shifting of peaks with La addition in BTS. Evidently, lattice parameter and unit cell volume decreased with increase of lanthanum doping in BTS. This is in accordance with smaller ionic radius of La^{3+} (1.36 Å) compared to Ba^{2+} (1.61 Å) which are reflective of successful substitution of La at the Ba site. The XRD pattern also indicates that the FWHM of the most intense diffraction peak ($2\theta = 31.5^\circ$) is getting broader with increase in La doping. This is indicative of a decrease in crystalline size with increased La addition.

Secondary electron images of $(\text{Ba}_{1-z}\text{La}_z)(\text{Ti}_{0.80}\text{Sn}_{0.20})\text{O}_3$ with ($z=0.00, 0.01, 0.02$ and 0.03) ceramic samples are shown in Fig 2 (a-d). Pure BTS sample (Fig. 2 (a)) reveals 3-dimensional

(3-D) grains with a size of 5-30 micro-meters. Many of the larger grains show terraced surface. Addition of La in BTS is found to inhibit grain growth. 1LBTS sample (Fig. 2 (b)) reveals grains of 0.5 to 2-micro-meters. 2LBTS sample (Fig. 2 (c)) clearly reveals a bimodal microstructure consisting 3-D submicron sized grains together with leafy (2-D) grains of the size of about 2-micrometers. Thus for 2 atomic % La doping, the growth of 3-D grains continues to be inhibited but nucleation and anomalous growth of 2-D (leafy) grains is observed. Thus 2 atomic % appears to be critical La doping level for the nucleation and growth of 2-D leafy grains. 3LBTS sample (Fig. 2 (d)) seems to be dominated by an extremely compact arrangement of leafy grains with a size of 2-5 micro-meters, which might be attributed to the higher La doping level as well as to the longer sintering time used for this sample. Thus, while a low La doping of 1 atomic % yielded inhibited grain growth in 1LBTS, higher amounts of La doping yield larger leafy grains in 2LBTS and 3LBTS. Similar results- grain growth inhibition at low La doping and enhanced grain growth at high La doping has been observed in La doped Ba(Zr,Ti)O₃ samples [13]. A systematic observation of microstructure of La doped BTS samples and mechanism of its formation has not been reported in the literature. Depending upon synthesis conditions, different competing doping mechanisms have been proposed. Formation of oxygen vacancies due to the addition of SnO₂ in BaTiO₃ has been reported [14]. Similarly, presence of unavoidable acceptor impurities has also been reported to yield O vacancies [15]. Oxygen vacancies are also known to result in samples annealed at high temperatures (> 1573 K) due to the evaporation of O [9]. The formation of large grains with terraced surfaces in BTS sample (Fig. 2 (a)) could be attributed to the enhanced mass transport via grain boundaries due to these O vacancies. With doping of La, the formation of O vacancies is suppressed [12] which might explain the inhibited grain growth at low La doping. For high La doping, addition of significant amount of La₂O₃ in the precursor

powder is likely to result in the lowering of melting point due to eutectic phenomenon [16]. The associated enhancement in the diffusion and mass transport explains the enhanced grain growth at high La doping. It has been reported that if the sintering temperature is not high enough, the grain surfaces may be approximated as atomically smooth structures and grain growth occurs by 2-D nucleation and lateral growth mechanism [16]. We propose that the mole fractions and sintering temperature of 1673 K for 2LBTS and 3LBTS samples are suitable for 2-D nucleation and lateral growth leading to formation and growth of leafy grains. In this way the peculiar grain growth pattern - inhibited grain growth at low La doping but enhanced and leafy grain growth for high La doping can be attributed to the combination of the following two competing factors: (i) suppression of O vacancies due to La doping leading to grain growth inhibition and (ii) enhancement of mechanism leading to nucleation and growth of 2-D (leafy) grains for La doping higher than 2 atomic % due to eutectic phenomena.

Room temperature Raman spectra of $(\text{Ba}_{1-z}\text{La}_z)(\text{Ti}_{0.80}\text{Sn}_{0.20})\text{O}_3$ with ($z=0.00,0.01,0.02$ and 0.03) are shown in Fig. 3. In a perfect cubic structure Raman modes are forbidden but broad Raman peaks are none the less obtained which is attributed to the disorder in the A or B sublattice [17] and to distorted oxygen octahedra [18-19]. The Raman spectra show six prominent modes and one anti resonance dip at 117, 192, 281, 506, 735, 836 and 141cm^{-1} respectively. These peaks, barring the one at 836cm^{-1} , match well with the reported data on Sn doped BaTiO_3 ceramics [20]. In particular, the intensity under the A_{1g} Transverse Optical mode at 506cm^{-1} was correlated with the formation and dynamics of polar nano-regions [20]. With increase in La doping the intensity under this peak increases indicating enhanced formation of polar nano regions. In the literature the peak close to 735cm^{-1} in Sn doped BTO samples have been interpreted differently by various authors. While Baskaran et al. [21] and Pokorny et al. [19]

have associated this peak to the ferroelectric breathing of BO_6 octahedra (tetragonal distortion) in the Sn doped BTO and pure BTO respectively, Kumar et al. [20] observed that it resembles the A_{1g} mode of classic relaxors associated with the breathing of BO_6 octahedra. It is worthwhile to compare it with the case of BZT, in which the peak at $\sim 715 \text{ cm}^{-1}$ is associated with ferroelectric breathing of BO_6 octahedra while the peak at $\sim 780 \text{ cm}^{-1}$ is associated with a A_{1g} stretching mode of BO_6 octahedra which becomes Raman active because of the presence of dissimilar B site species at the centre of octahedra [19, 21-22]. On increasing La doping in BZT, the peak intensity under A_{1g} mode increases [18]. In the present work however, the most noticeable change due to La doping in BTS is the appearance of peak at 839 cm^{-1} . It has been reported that La doping in pure BTO also results in the appearance of the A_{1g} relaxor phase peak at 840 cm^{-1} which was attributed to the Ti vacancies created at B sites due to La doping at A sites [21]. In view of the preceding discussion it is proposed that the peak at 735 cm^{-1} in BTS and LBTS is associated with the ferroelectric breathing of tetragonal BO_6 octahedra and the peak at 839 cm^{-1} is associated with the A_{1g} stretching mode of BO_6 octahedra which is characteristic of relaxor phase. This raises the question as to why the A_{1g} mode is absent in BTS but present in BZT. The explanation for this could be the similar ionic radii of Sn^{4+} (0.71 \AA) and Ti^{4+} (0.68 \AA); the ionic radius of Zr^{4+} on the other hand is much larger (0.79 \AA).

Temperature dependent dielectric permittivity (ϵ) and loss factor ($\tan \delta$) at different frequencies of sintered $(\text{Ba}_{1-z}\text{La}_z)(\text{Sn}_{0.20}\text{Ti}_{0.80})\text{O}_3$ with ($z= 0.00, 0.01, 0.02$ and 0.03) ceramics are shown in Fig. 4. A significant increase in full width at half maxima (FWHM) along with decrease in maximum dielectric permittivity (ϵ_m) and Curie temperature (T_c) with increase of La doping has been reported [11]. The extent of relaxor ferroelectricity characteristics is parameterized by the *exponent* γ in the modified Curie-Weiss law; [24-25]

$$\frac{1}{\epsilon} - \frac{1}{\epsilon_m} = \frac{(T-T_m)^\gamma}{C}, (T > T_m) \quad (1)$$

Where T_m is the temperature corresponding to the dielectric permittivity maximum, C is the Curie constant, ϵ_m is the peak dielectric permittivity at temperature T_m and exponent γ reflects the nature of relaxor phase transition. Inverse dielectric constant plots as function of temperature at 100 kHz are shown in Fig. 5. The inset in each panel shows plots of $\ln(1/\epsilon - 1/\epsilon_m)$ verses $\ln(T-T_m)$ for all compositions, the slopes of which determine the exponent γ . The experimental data were fitted to equation (1) and the best-fit values for T_m , ϵ_m , and γ were obtained at frequency 100 kHz. Further, $\delta T_{\text{relax}} = T_m(1 \text{ MHz}) - T_m(1 \text{ kHz})$ and Full width at half maxima (FWHM) were also determined. All these values are summarized in Table 1 that is discussed below.

As seen in Fig. 4 (a and b), BTS and 1LBTS samples do not show noticeable shift in dielectric peak transition temperature (T_m) with increasing frequency as δT_{relax} are found to be 0 K and 4 K respectively. It is however worth noting that even 1 atomic % of La doping in BTS has resulted in marked increase in the FWHM of the phase transition (Table 1) and the value of maximum dielectric constant is less sensitive to the applied frequency (Fig. 4 (b)). This negligible frequency dispersion and broad peak is signature of ferroelectricity with *diffused* phase transition. On the other hand, significantly higher dielectric dispersion, $\delta T_{\text{relax}} = 10 \text{ K}$ and 16 K , is observed for La doping ($z = 0.02$ and 0.03 respectively) in Fig. 4 (c, d). Thus we conclude that 2 atomic % of La doping is able to induce relaxor behaviour in BTS20 sample. In comparison δT_{relax} of 10 K was obtained in BTS15 sample for a La doping of 3 atomic % [11]. In contrast, it is reported that in the absence of La doping, the Sn doping would have to be increased to 30 atomic % to induce relaxor behaviour in pure Barium Titanate [26]. As has been well documented in the literature [12-13] substitution of La^{3+} (ionic radius 1.32 \AA) in place of Ba^{2+}

(ionic radius 1.61 Å) introduces Ti vacancies or Ti^{3+} in the lattice. This disorder introduces random electric fields and strain because of which polar nano regions are induced. The flipping or the breathing of polar nano-regions is considered to be responsible for the relaxor properties [27].

From equation 1, it is clear that in normal ferroelectric transition, $\gamma=1$ while for complete relaxor behaviour ~ 2 and an incomplete-diffused phase or relaxor phase transition, $1 \leq \gamma \leq 2$ [28]. It is observed that as La addition increases from $z=0.00, 0.01, 0.02$ and 0.03 , the γ increases from 1.42, 1.88, 2.017 and 2.018 respectively. This conclusively proves that La addition onto BTS drives the system into a robust relaxor phase. Although the broadening (with respect to temperature) of the phase transition is achieved by La doping, the maximum dielectric constant has actually decreased. This decrease could be attributed to the increased volume fraction of grain boundaries, due to decrease in grain size (Fig. 2). Similar decrease in dielectric constant and grain size on La doping has been reported in BST [12] and BZT [13]. For the high dielectric constant capacitor applications, while the broadening of the phase transition has been achieved, the dielectric constant needs to be enhanced by increasing grain size and controlling oxygen vacancies. Indeed, the 3LBTS, whose microstructure comprises of a compact arrangement of relatively larger 2D (leafy) grains, shows a slight enhancement in the dielectric constant although the FWHM has also correspondingly decreased (Fig. 4 and Table 1).

We note that the temperature of the loss maxima as well as the dielectric loss peak value increases with increase in frequency. Similar behaviour was observed in La doped BZT [13] and La doped BTS [12]. The dielectric loss values at room temperature and 10 kHz are however higher than those in La doped BZT [13]. This could be due to conductive dielectric losses due to oxygen vacancies in Sn doped BT samples [12].

Polarization (P) versus Electric field (E) hysteresis loops at room temperature for all the samples are shown in Fig. 6. The remnant polarization and coercive field for BTS, 1LBTS, 2LBTS and 3LBTS are listed in Table 2. In pure BTS, some measure of saturation in polarization is observed, but full saturation was not obtained even after increasing E to 30 kV/cm. The PE loops for La doped samples do not show saturation indicating the presence of pinned polar nano-regions [12]. Since T_m decreases with increase in La doping, it is expected that the PE loops obtained at fixed room temperature would also become slimmer with increase in La doping. However coercive field in 2LBTS is only marginally smaller than in 1LBTS. This might be attributed to enhanced grain boundary pinning due to small grain size in 2LBTS [29]. In addition, pinning due to oxygen vacancies arising due to oxygen loss might also play a role [14].

4. Conclusions

In conclusion, we report a detailed microstructural and dielectric characterization of a series of lanthanum doped barium stannate titanate ceramics. The samples were prepared by solid state reaction technique and XRD analysis indicated single phase microstructure. SEM images indicated that while a low La doping of 1 atomic % yielded inhibited grain growth in 1LBTS, higher amounts of La doping yield larger leafy grains. This peculiar grain growth and microstructure evolution can be attributed to the combination of the following two competing factors: (i) suppression of O vacancies due to La doping leading to grain growth inhibition and (ii) enhancement of mechanism leading to nucleation and growth of 2-D (leafy) grains for La doping higher than 2 atomic % due to eutectic phenomena. Dielectric permittivity measurements indicate that 1 atomic % of La enhances diffuse phase transition in $\text{Ba}(\text{Ti}_{0.80}\text{Sn}_{0.2})\text{O}_3$, but the frequency dependence of T_m is observed only at 2 atomic % of La doping. This relaxor behaviour, the increase in the intensity of Raman peaks with increase in La doping, as well as the

non-saturated PE hysteresis loops in La doped BTS indicate the presence of polar nano-regions. The decreased dielectric permittivity of La doped BTS can, at least partially, be attributed to the reduced grain size. The ferroelectric coercivity of 2LBTS is only marginally smaller in comparison to 1LBTS which could be explained on the basis of pinning due to grain boundaries and oxygen vacancies in 2LBTS. For the high dielectric constant capacitor applications, while the broadening of the phase transition has been achieved, the dielectric constant needs to be enhanced further by increasing the grain size and controlling oxygen vacancies.

5. Acknowledgements

Authors thank Dr. Satyendra Singh from SCNS, JNU, New Delhi, for access to PE loop tracer and Advance Instrument Research Facility AIRF, JNU, New Delhi, India, for access to SEM.

B.B. acknowledges financial support via UGC start-up grant and DST Purse grant.

6. References

- [1] T. Shi, L. Xie, L. Gu, J. Zhu, Why Sn doping significantly enhances the dielectric properties of $\text{Ba}(\text{Ti}_{1-x}\text{Sn}_x)\text{O}_3$, *Scientific Reports*, 5 (2015) 8606.
- [2] K. Uchino, *Ferroelectric Devices*, second edition, Taylor & Francis, New York, 2010.
- [3] G.A. Samara, The relaxational properties of compositionally disordered ABO_3 perovskites, *Journal of Physics: Condensed Matter*, 15 (2003) R367.
- [4] F. Jona, G. Shirane, *Ferroelectric crystals*, Dover Publications, New York, 1993.
- [5] Y. Liu, R. Withers, B. Nguyen, K. Elliott, Structurally frustrated polar nanoregions in BaTiO_3 -based relaxor ferroelectric systems, *Applied physics letters*, 91 (2007) 152907.
- [6] G. Smolensky, V. Isupov, Phase transitions in some solid solutions with ferroelectric properties, in: *Dokl Akad Nauk SSSR*, 1954, pp. 53-54.
- [7] G.H. Haertling, Ferroelectric ceramics: history and technology, *Journal of the American Ceramic Society*, 82 (1999) 797-818.
- [8] X. Wei, X. Yao, Preparation, structure and dielectric property of barium stannate titanate ceramics, *Materials Science and Engineering: B*, 137 (2007) 184-188.
- [9] F.D. Morrison, D.C. Sinclair, A.R. West, Doping mechanisms and electrical properties of La-doped BaTiO_3 ceramics, *International Journal of Inorganic Materials*, 3 (2001) 1205-1210.
- [10] A.R. West, T.B. Adams, F.D. Morrison, D.C. Sinclair, Novel high capacitance materials:- BaTiO_3 : La and $\text{CaCu}_3\text{Ti}_4\text{O}_{12}$, *Journal of the European Ceramic Society*, 24 (2004) 1439-1448.
- [11] S.K. Upadhyay, V.R. Reddy, P. Bag, R. Rawat, S. Gupta, A. Gupta, Electro-caloric effect in lead-free Sn doped BaTiO_3 ceramics at room temperature and low applied fields, *Applied physics letters*, 105 (2014) 112907.
- [12] S. Singh, P. Singh, O. Parkash, D. Kumar, Structural and relaxor behavior of $(\text{Ba}_{1-x}\text{La}_x)(\text{Ti}_{0.85}\text{Sn}_{0.15})\text{O}_3$ ceramics obtained by solid state reaction, *Journal of Alloys and Compounds*, 493 (2010) 522-528.
- [13] X. Chou, J. Zhai, X. Yao, Relaxor behavior and dielectric properties of La_2O_3 -doped barium zirconium titanate ceramics for tunable device applications, *Materials Chemistry and Physics*, 109 (2008) 125-130.
- [14] I. Souza, L. Cavalcante, J. Sczancoski, F. Moura, C. Paiva-Santos, J.A. Varela, A.Z. Simões, E. Longo, Structural and dielectric properties of $\text{Ba}_{0.5}\text{Sr}_{0.5}(\text{Sn}_x\text{Ti}_{1-x})\text{O}_3$ ceramics obtained by the soft chemical method, *Journal of Alloys and Compounds*, 477 (2009) 877-882.
- [15] D. Smyth, The role of impurities in insulating transition metal oxides, *Progress in solid state chemistry*, 15 (1984) 145-171.
- [16] W. Jo, U.-J. Chung, N.-M. Hwang, D.-Y. Kim, Temperature dependence of the coarsening behavior of (Ba, Sr) TiO_3 grains dispersed in a SiO_2 -rich liquid matrix, *Journal of the European Ceramic Society*, 23 (2003) 1565-1569.
- [17] N. Karan, R. Katiyar, T. Maiti, R. Guo, A. Bhalla, Raman spectral studies of Zr^{4+} -rich $\text{Ba}(\text{Zr}_x\text{Ti}_{1-x})\text{O}_3$ ($0.5 \leq x \leq 1.00$) phase diagram, *Journal of Raman Spectroscopy*, 40 (2009) 370-375.
- [18] S. Ghosh, M. Ganguly, S. Rout, T. Sinha, Order-disorder correlation on local structure and photo-electrical properties of La^{3+} ion modified BZT ceramics, *The European Physical Journal Plus*, 130 (2015) 1-18.

- [19] J. Pokorný, U. Pasha, L. Ben, O. Thakur, D. Sinclair, I. Reaney, Use of Raman spectroscopy to determine the site occupancy of dopants in BaTiO₃, *Journal of Applied Physics*, 109 (2011) 114110.
- [20] A. Kumar, I. Rivera, R. Katiyar, Investigation of local structure of lead-free relaxor Ba(Ti_{0.70}Sn_{0.30})O₃ by Raman spectroscopy, *Journal of Raman Spectroscopy*, 40 (2009) 459-462.
- [21] N. Baskaran, H. Chang, Effect of Sn doping on the phase transformation properties of ferroelectric BaTiO₃, *Journal of Materials Science: Materials in Electronics*, 12 (2001) 527-531.
- [22] V. Buscaglia, S. Tripathi, V. Petkov, M. Dapiaggi, M. Deluca, A. Gajović, Y. Ren, Average and local atomic-scale structure in Ba(Zr_xTi_{1-x})O₃ (x= 0.10, 0.20, 0.40) ceramics by high-energy X-ray diffraction and Raman spectroscopy, *Journal of Physics: Condensed Matter*, 26 (2014) 065901.
- [23] V.S. Puli, A. Kumar, D.B. Chrisey, M. Tomozawa, J. Scott, R.S. Katiyar, Barium zirconate-titanate/barium calcium-titanate ceramics via sol-gel process: novel high-energy-density capacitors, *Journal of Physics D: Applied Physics*, 44 (2011) 395403.
- [24] H. Martirena, J. Burfoot, Grain-size and pressure effects on the dielectric and piezoelectric properties of hot-pressed PZT-5, *Ferroelectrics*, 7 (1974) 151-152.
- [25] K. Uchino, S. Nomura, Critical exponents of the dielectric constants in diffused-phase-transition crystals, *Ferroelectrics*, 44 (1982) 55-61.
- [26] W. Xiaoyong, F. Yujun, Y. Xi, Dielectric relaxation behavior in barium stannate titanate ferroelectric ceramics with diffused phase transition, *Applied physics letters*, 83 (2003) 2031-2033.
- [27] C. Lei, A. Bokov, Z. Ye, Ferroelectric to relaxor crossover and dielectric phase diagram in the BaTiO₃-BaSnO₃ system, *Journal of Applied Physics*, 101 (2007) 84105-84105.
- [28] X. Diez-Betriu, J. Garcia, C. Ostos, A. Boya, D. Ochoa, L. Mestres, R. Perez, Phase transition characteristics and dielectric properties of rare-earth (La, Pr, Nd, Gd) doped Ba(Zr_{0.09}Ti_{0.91})O₃ ceramics, *Materials Chemistry and Physics*, 125 (2011) 493-499.
- [29] W. Cai, C. Fu, J. Gao, H. Chen, Effects of grain size on domain structure and ferroelectric properties of barium zirconate titanate ceramics, *Journal of Alloys and Compounds*, 480 (2009) 870-873.

Figure captions

FIGURE 1. (Colour online) Room temperature XRD patterns of ceramic powder: (a) BTS (b) 1LBTS (c) 2LBTS (d) 3LBTS. Portion ($36 \leq 2\theta \leq 47$) of the XRD plot is shown magnified in inset.

FIGURE 2. Scanning electron microscopy (SEM) images of ceramics pellets: (a) BTS (b) 1LBTS (c) 2LBTS (d) 3LBTS.

FIGURE 3. (Colour online) Room temperature Raman spectra recorded from ceramics pellets: (a) BTS (b) 1LBTS (c) 2LBTS (d) 3LBTS.

FIGURE 4. (Colour online) Temperature dependent dielectric permittivity of ceramics pellets: (a) BTS (b) 1LBTS (c) 2LBTS (d) 3LBTS.

FIGURE 5. (Colour online) Plot of inverse dielectric constant at 100 kHz as function of temperature of ceramic pellets: (a) BTS (b) 1LBTS (c) 2LBTS (d) 3LBTS. Inset shows the corresponding $\ln(1/\epsilon - 1/\epsilon_m)$ versus $\ln(T - T_m)$. Linear fittings in the high temperature regime are indicated by solid lines.

FIGURE 6. (Colour online) Room temperature Polarization (P) versus Electric Field (E) hysteresis loop of ceramic pellets: (a) BTS, (b) 1LBTS, (c) 2LBTS, (d) 3LBTS.

Table captions

Table 1. The values of T_m , ϵ_m and γ obtained from modified Curie–Weiss Law and FWHM values of the ϵ (T) at 100 kHz are given: (a) BTS, (b) 1LBTS, (c) 2LBTS, (d) 3LBTS.

Table 2. Coercive field (E_c) and remnant polarization (P_r) of ceramic pellets are given: (a) BTS, (b) 1LBTS, (c) 2LBTS, (d) 3LBTS.

Table 1

La Doping	$z=0.0$	$z=0.01$	$z=0.02$	$z=0.03$
$T_m(\text{K})$	238	204.8	146.8	121.5
$\epsilon_m(\text{F/m})$	7361	3727	1333	2182
$\delta T_{\text{relax}} = T_m$ (1 MHz) — T_m (1 kHz)	0	4	10	16
FWHM calculated (at 100 kHz)	36	85	115	90
γ	1.42	1.88	2.017	2.018

Table 2

La doping	Remnant Polarization P_r ($\mu\text{C}/\text{cm}^2$)	Coercive Electric Field E_c (kV/cm)
$z=0.00$	0.70	3.92
$z=0.01$	0.50	2.75
$z=0.02$	0.147	2.71
$z=0.03$	0.095	1.22

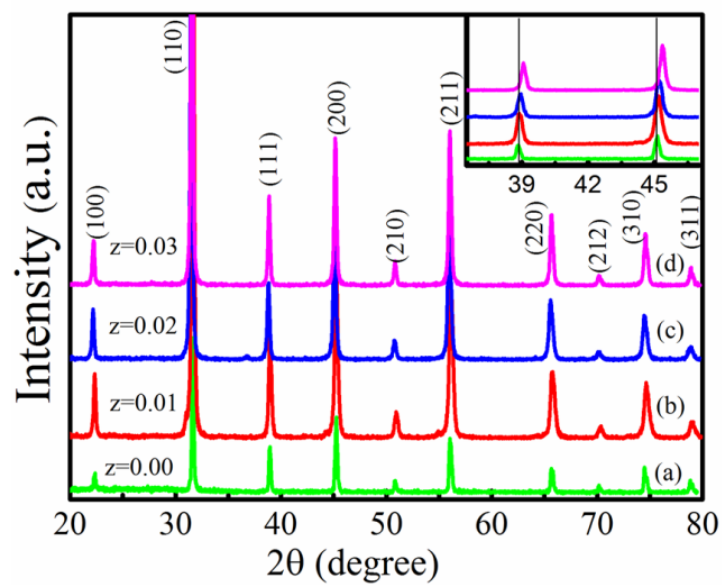


FIGURE 1.

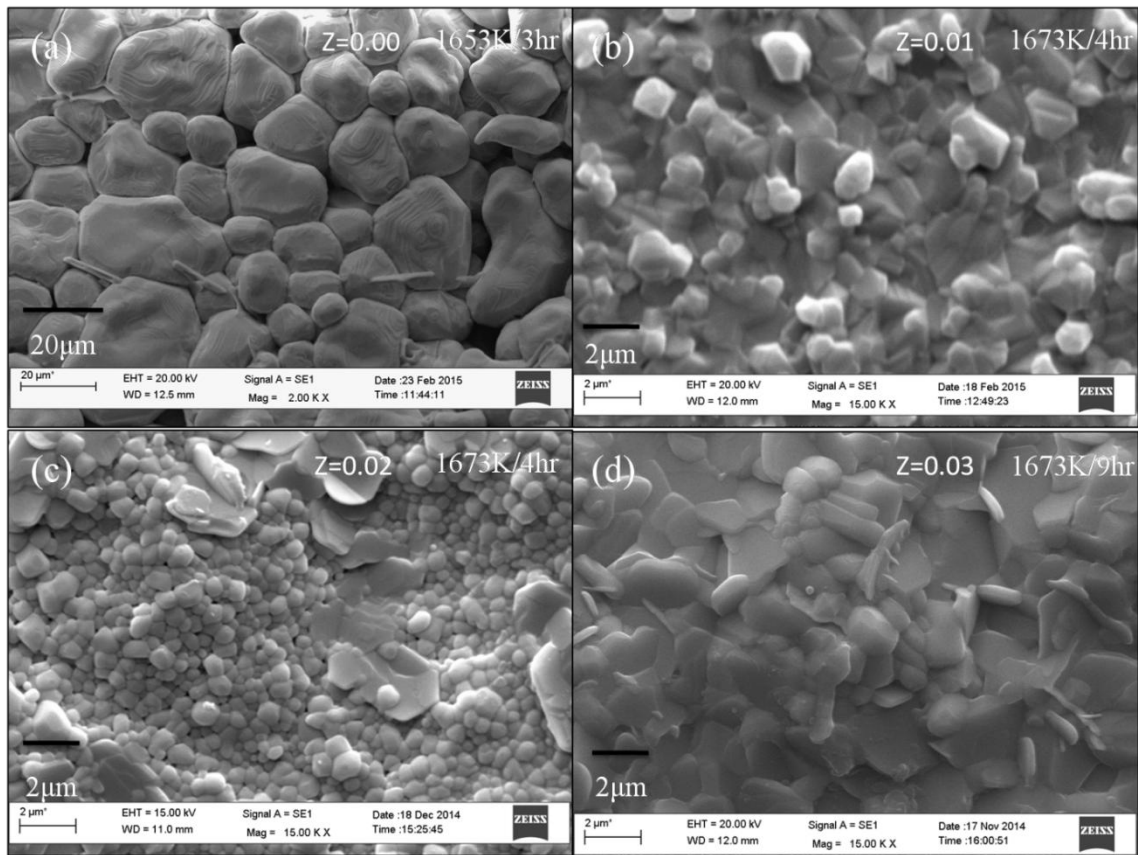


FIGURE 2.

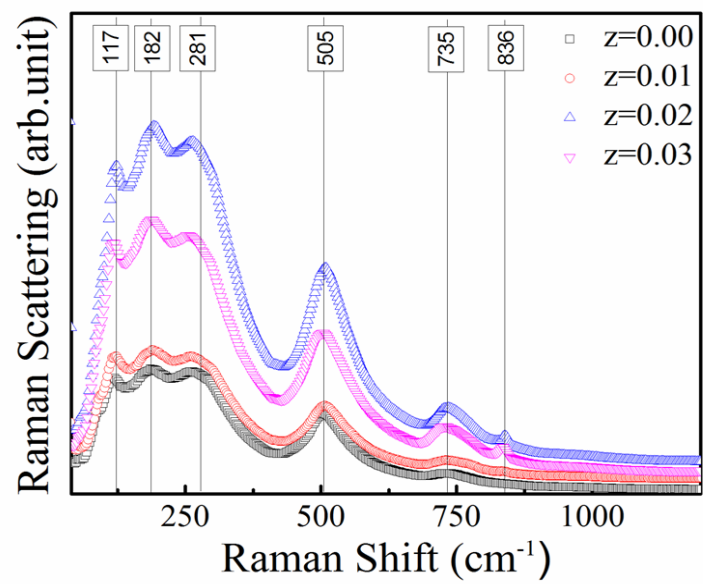


FIGURE 3.

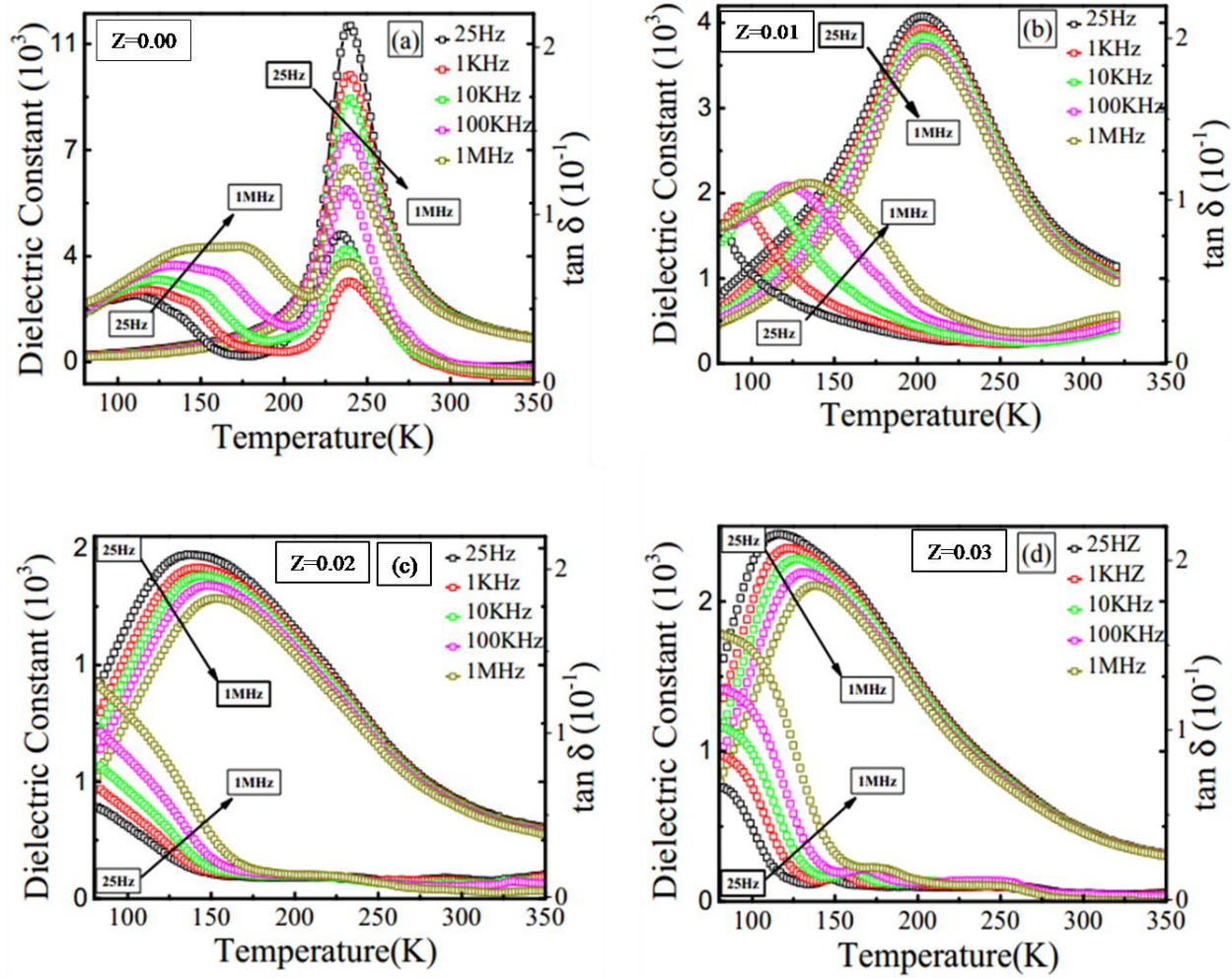


FIGURE 4.

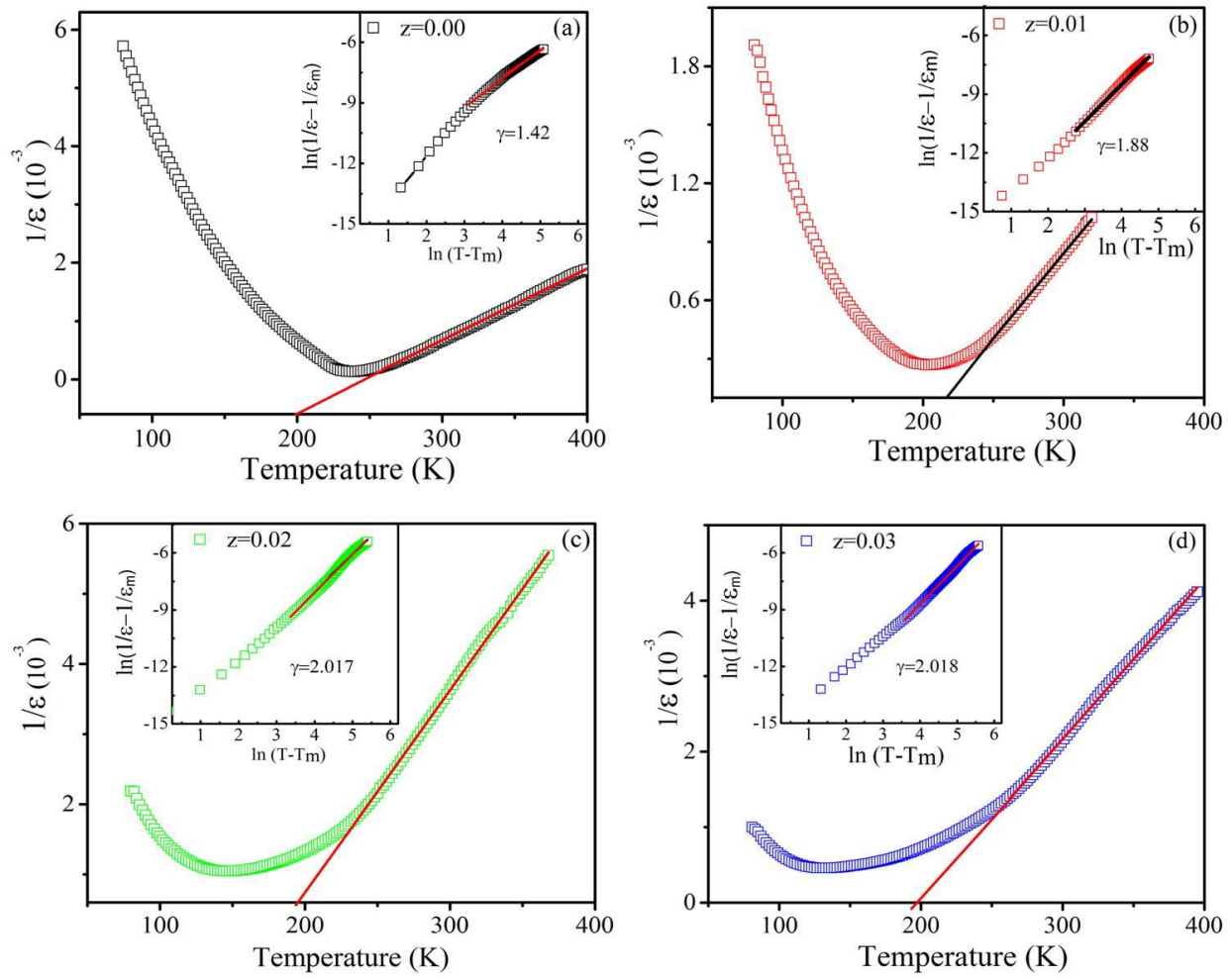


FIGURE 5.

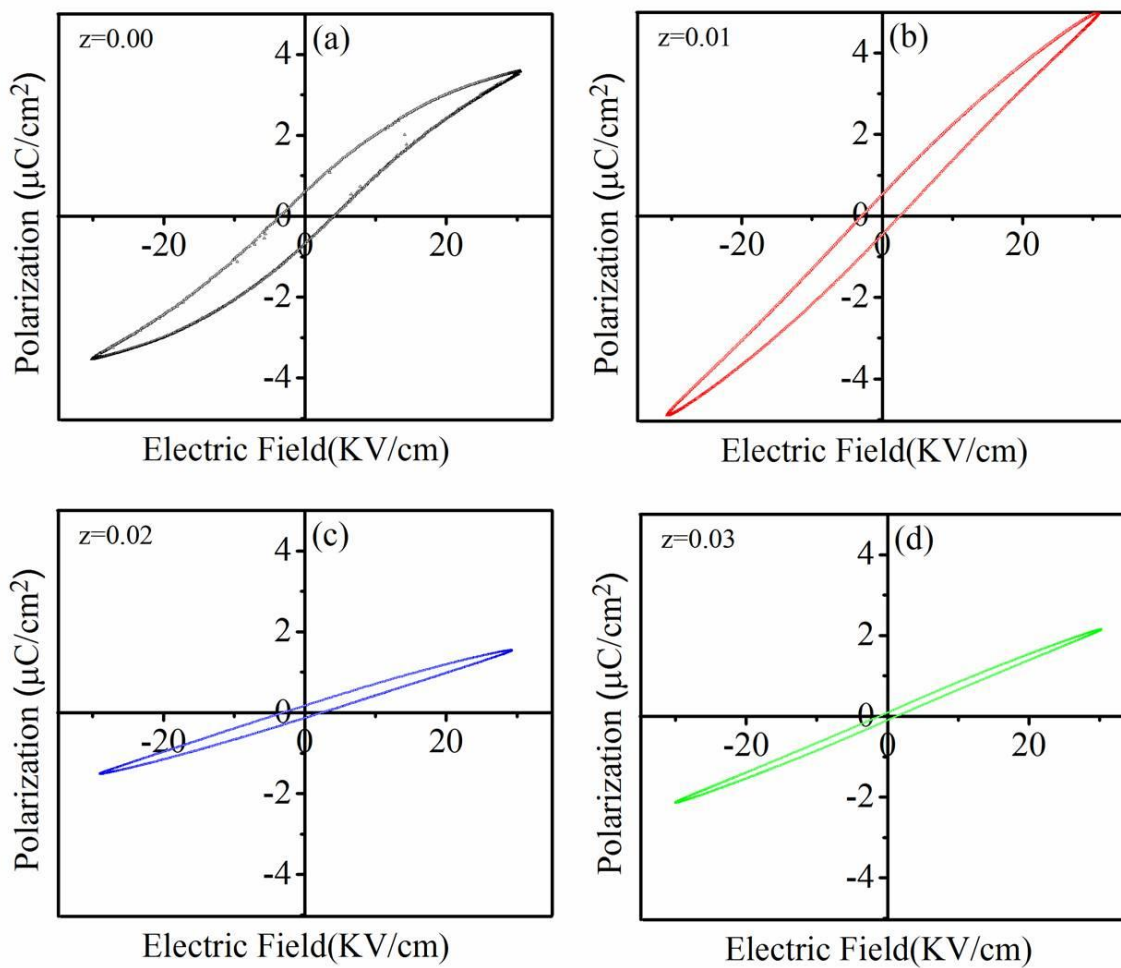


FIGURE 6.